Journal of
Ceramic Science
and Technology

J. Ceram. Sci. Technol., **14** [2] 89-98 (2023)
DOI: 10.4416/JCST2023-00009
available online at: http://www.ceramic-science.com

Influence of Sintering Parameters on the Structure of Alumina Tubular Membranes Obtained by Freeze-Casting

P. Cristh Fonseca Alves*[1], D. Guimarães da Silva[1], D. Cordeiro Leite Vasconcelos[1], W.L. Vasconcelos[1], J. Ferreira do Nascimento[2], D. Carrijo de Melo[2], L. dos Santos Pereira[2]

[1]Department of Metallurgical and Materials Engineering, Federal University of Minas Gerais - UFMG, Avenida Presidente Antônio Carlos, 6627, Campus UFMG, Escola de Engenharia, bloco 2, sala 2233, Belo Horizonte, MG, CEP: 31270 – 901, Brazil.
[2]Petrobras/CENPES, Avenida Horácio Macedo 950, Cidade Universitária, Ilha do Fundão, Rio de Janeiro, RJ, CEP: 21941 – 915, Brazil.

received July 3, 2023; received in revised form September 11, 2023; accepted September 25, 2023

Abstract

This study compares for the first time the influence of different sintering routes on the structure of alumina samples prepared with the freeze-casting technique. Two-stage and fast sintering routes were compared with the conventional sintering route, and the sintering program proved to be crucial in controlling the microstructure of alumina ceramics. The results suggest that the alumina porosity and particle size are highly dependent on the sintering route. It was observed that the two-step sintering route is more efficient in controlling the particle growth of alumina (0.8 μm) when compared to the conventional (1.2 μm) and fast (0.9 μm) sintering routes. Regarding the mechanical properties, it was observed that an improvement in flexural strength was achieved when the two-stage sintering program (6.15 MPa) was used, which is associated with its microstructural refinement.

Keywords: Freeze-casting, alumina tubes, sintering, membranes

I. Introduction

Different forming techniques can be used in the industrial production of tubular-shaped ceramics; these techniques include extrusion, slip casting, uniaxial pressing. Each of these methods has its own merits and drawbacks, but all of them result in final products with random porosity [1]. Freeze-casting, also called ice-templating, is an emerging technology to produce hierarchically porous ceramics with aligned and directional pores. Furthermore, the freeze-cast samples can exhibit a wide range of porosity (30 – 99 %) which can be controlled based on the suspension concentration and processing parameters [1,2].

The freeze-casting technique consists of freezing a stable ceramic slurry basically composed of a ceramic powder, a solvent (aqueous or not) and additives (organic binders and dispersants). The inorganic particles dispersed in the suspension are expelled by the moving solidification front and piled up between the growing solvent crystals. The freezed solvent is then sublimated at low pressures, creating pores in the material. The as-generated pores are a replica of the solvent crystals. Therefore, a large range of pore configurations can be obtained by changing the solvent, since each solvent has a specific geometry when solidified. The ceramic green bodies are then heat-treated to consolidate their structure [1,2].

* Corresponding author: priscilacristhfa@gmail.com

Owing to the versatility of the process, the porous materials obtained with the freeze-casting technique have wide application potential in different technologies, such as supports for membranes in the petrochemical industry (oil/water separation [3,4] as well as in natural gas purification [5,6]), solid oxide fuel cells (SOFC) and as catalysts. Furthermore, freeze-casting can be used for obtaining piezoelectric materials, porous ceramics for thermal insulation applications and biomaterials [7].

After the ceramic forming process, the material obtained is called a "green body". In the green body state, the inorganic particles are connected by weak bonds, usually created by the organic binder added in the slurry preparation step. To transform the shaped powder into a resistant solid structure, the green body undergoes a heat treatment step known as sintering. The transition from the fragile green-body state to a resistant solid structure occurs through the formation of bonds between the inorganic particles, which can only occur in heat treatment at high temperatures. The bonds created in the sintering process lead to a ceramic material with greater mechanical strength [8].

The sintering process can be generally divided into three stages called the initial, intermediate and final stages. Fig. 1 schematically represents the heat treatment process for a ceramic green body obtained by means of freeze-casting. In the initial sintering stage, also known as the "neck

growth stage", diffusion begins to occur at the edges of the contacting particles and necks are formed between adjacent particles. The driving force of neck formation is the reduction of the surface area between the particles and the subsequent reduction of the system free energy. Mass transport in this case occurs mainly by the surface diffusion mechanism [9,10].

In the intermediate sintering stage, the particles start to grow and the volume of the pores and pore channels (created by the ice crystals solidification during the freezing step) start to shrink due to the material densification. The impingement of the necks upon each other causes the rupture of some pore channels, forming disconnected and isolated pores. At the same time, the particles begin to grow. The transport mechanisms of the intermediate stage are mainly particle boundary diffusion, surface diffusion and volumetric diffusion [9].

The last sintering stage is slower than the intermediate stage. In the final stage, there is an increase in the average particle size of the ceramic particles and the pores become smaller and spherical. Smaller pores and pore channels are eliminated during this step [9, 10].

The heat treatment step can be carried out in ambient pressure or with the application of pressure, however, pressureless sintering is often preferable owing to lower costs. A conventional way of sintering under ambient pressure is to heat the sample to an elevated temperature, holding this temperature for some time and then cooling it to room temperature. However, many authors have reported that heating ceramic specimens using slow heating rates and long dwell times can induce the phenomenon of exaggerated particle growth. In general, the mechanical strength of ceramic materials decreases significantly with increasing average particle size [11, 12, 13].

Special sintering step control processes are reported as strategies capable of refining the microstructure and improving the mechanical properties of the final product, compared to conventional sintering. Examples of variation in the ambient pressure sintering process are rate-controlled sintering, two-step sintering and the rapid-rate sintering method [12, 14, 15].

Rapid-rate sintering, also called fast-firing, has been applied to green ceramics with the aim of improving the microstructure of the final products as well as saving time and/or energy. With the rapid-rate sintering method, samples are rapidly heated to the desired temperature, followed by subsequent cooling to room temperature without isothermal dwell [16, 17]. Esposito and Traversa [18] investigated the heat treatment of ceramic pellets obtained with ceria doped with nanometric samaria (SDC) and ceria doped with gadolinium (GDC) by the fast-firing sintering method. It was observed that the samples heat-treated by means of fast-firing showed reduced granulometry in comparison with conventionally sintered samples.

Another variation in heat treatment is the two-stage sintering method, initially proposed by Chen and Wang in 2000 [13]. The first stage consists of heating the samples to a high temperature, when the material reaches an intermediate porosity, and the second stage consists of rapid cooling to a lower temperature with an isothermal dwell at that lower temperature for a specified time. Fast cooling to a lower temperature suppresses particle growth and allows densification to occur at a lower temperature. Isobe *et al.* [19] prepared porous Al_2O_3 ceramics with the slip-casting technique and the heat treatment was performed with the two-stage sintering method. The authors reported success in controlling pore size by modifying the sintering time in the second step of the two-stage method, without changing the final porosity. Bodišová *et al.* [12] reported success in retarding particle growth in the final stage of sintering of alumina ceramics obtained by means of uniaxial pressing. Lóh *et al.* [20] also obtained alumina ceramics by uniaxial pressing and the study revealed that the two-step sintering technique gives rise to materials with smaller average particles size, when compared to conventional sintering. Studies employing two-step sintering on alumina ceramics and other oxides were summarized by Lóh *et al.* [21]. The microstructure refinement obtained by using sintering control in barium titanate materials produced by freeze-casting was described by Xu and Wang [22].

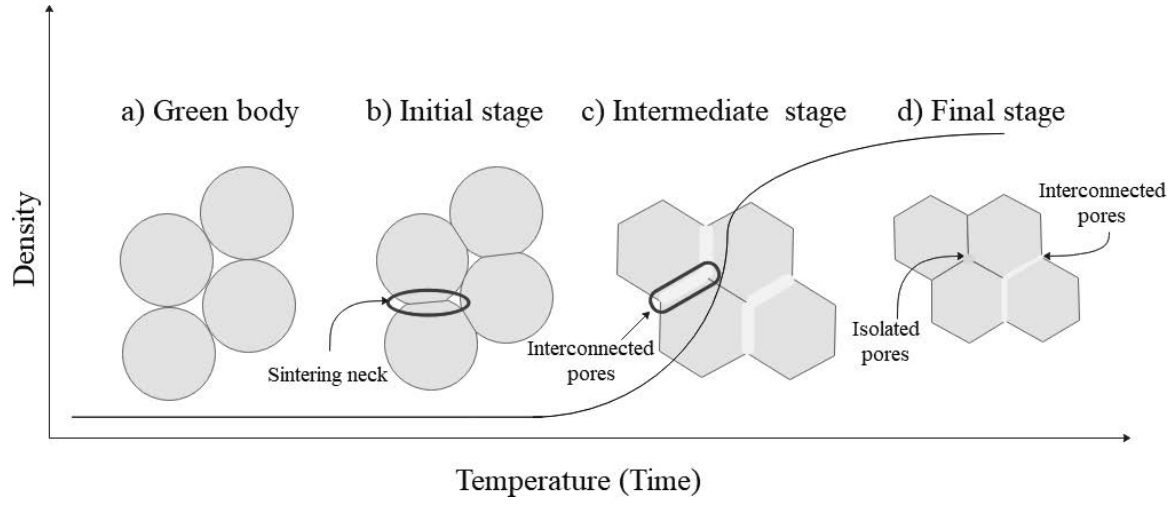

Fig. 1: Schematic diagram of the sintering process of a) green body b) initial stage; c) intermediate stage and d) final stage.

Although many studies reporting the use of sintering control in the heat treatment of ceramics have been published, this control has not yet been discussed for porous alumina obtained by means of freeze-casting. In this context, the use of the technique deserves analysis, mainly for comparison with the use of conventional sintering at ambient pressure.

The aim of this study is to investigate the influence of sintering control on the microstructure and mechanical properties of alumina samples obtained by freeze-casting. Two different heat treatment routes (rapid-rate sintering and two-stage sintering) were applied to the specimens and the results were compared with the alumina samples obtained with the conventional sintering technique.

II. Experimental Procedure

(1) Materials and methods

The production of ceramic samples by means of the freeze-casting process was carried out in several steps, as illustrated in Fig. 2. First, aqueous suspensions (100 mL) were prepared by dispersing 20 vol% Al_2O_3 powder with an average particle size of 0.5 µm in deionized water, with 1 % by weight of ammonium polymethacrylate anionic dispersant and 2 wt% polyvinyl alcohol binder. The prepared suspension was sonicated to remove air bubbles.

The slurry obtained was then poured into a tubular copper mold. The filled mold was immersed in a liquid nitrogen bath and kept in this until complete freezing. The frozen alumina samples were freeze-dried in a Liotop L101 series freeze dryer until complete solvent sublimation. The as-prepared green bodies were heat-treated in air using a muffle furnace. Obtained were 50-mm-long samples with inner and outer diameters measuring about 6.5 mm and 10 mm, respectively.

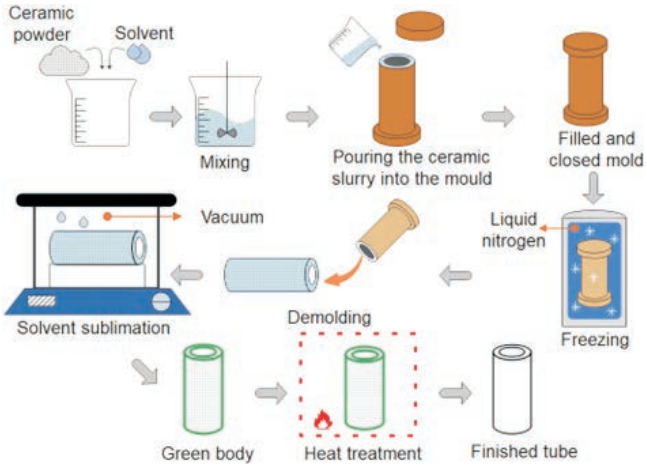

Fig. 2: Schematic diagram of freeze-casting steps.

As mentioned earlier, different sintering routes were used in this study, as schematically illustrated in Fig. 3 a-d. Prior to sintering, all samples were preheated to 550 °C at a heating rate of 2 K/min and maintained for 1 hour (t_1) isothermal plateau to ensure complete removal of organic matter. In the conventional sintering routes SR 1 (Fig. 3a) and SR 2 (Fig. 3b), the alumina samples were heated to 1 500 °C and 1 600 °C at a heating rate of 2 K/min, respectively, and kept constant at this temperature for 1 hour (t_2). For the SR 3 two-stage sintering route (Fig. 3c), the green samples were heated to 1 600 °C at a heating rate of 2 K/min, then cooled down to the temperature of 1 500 °C and held at this temperature for 1 hour (t_2). For the fast-sintering route SR 4 (Fig. 3d), the specimens were heated up to the maximum temperature of 1 600 °C and then immediately, without isothermal dwell, cooled down to room temperature. The cooling rate for all samples was 5 K/min.

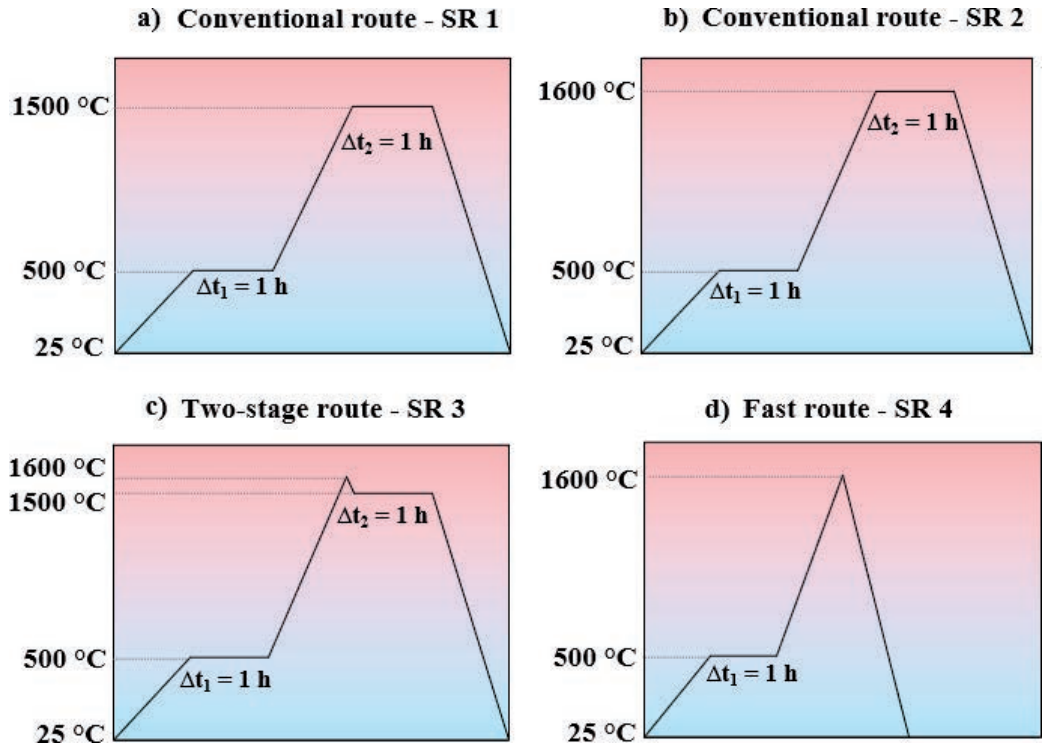

Fig. 3: Schematic illustration of the a) SR 1, b) SR 2, c) SR 3 and SR 4 sintering routes.

(2) Characterization

The porosity of the sintered samples was measured by means of water immersion (Archimedes' principle) according to the ASTM (American Society for Testing and Materials) B962 – 17 [23] and C20 – 00 [24] standards. The samples were cut and coated with a thin carbon layer for scanning electron microscopy analysis (Jeol JSM - 6360 LV) in order to investigate their microstructure. An estimate of alumina particles' average diameter for samples sintered using different sintering profiles was carried out using the Image J software, which is in the public domain. At least 200 particle dimension measurements were conducted for each scanning electron microscope image, in order to obtain a statistically robust set of data. The same protocol was adopted for pore size measurements. The samples' linear shrinkage (L_s) was assessed considering their diameter dimensions before (L_0) and after (L_1) the heat treatment, according to Equation 1: 0

$$L_s = \left(\frac{L_1 - L_0}{L_0} \right) \times 100 \quad (1)$$

The mechanical strength of the samples was evaluated in three-point bending tests. The maximum bending strength (σ) was obtained using Equation 2 [25]:

$$\sigma = \frac{8FLd_o}{\pi \left(d_o^{\,4} - d_i^{\,4} \right)} \quad (2)$$

where F represents the force at the fracture; d_o and d_i refers to the outer and inner diameter of the samples respectively; and L is the distance between the two outer rollers (30 mm). The mechanical tests were performed at room temperature with a constant compression rate of 0.5 mm·min^{-1} using an INSTRON EMIC 2310 (software: Blue Hill, Universal Testing Machine).

III. Results and Discussion

A typical microstructure of the alumina green body is shown in Fig. 4. A good dispersion of Al_2O_3 particles can be observed in the SEM images, as well as their contacts provided by the organic binder and the formation of circular pores as result of the typical geometry resulting from the solvent (H_2O) solidification.

The outer surface of freeze-cast samples sintered using the SR 1 and SR 3 routes (longitudinal section view, parallel to the freezing direction) is shown in the SEM micrographs in Fig. 5a-b. In Fig. 5, it is possible to observe the presence of sintering necks and connections between alumina particles, which were non-existent in the green body (Fig. 4), and also reduced porosity. The driving force for coarsening of polycrystalline materials is the reduction in the particles' boundary area because of particle growth. At the particles' boundary, the surfaces become more "curved" as a result of surface chemical potential changes in processes such as particle growth, particle boundary migration, porosity reduction, etc. [18].

The conventional sintering process conducted in the SR 1 route (Fig. 5a) led to a structure with connected Al_2O_3 particles and a network of pores. The use of the two-stage route SR 3 (Fig. 5b) produced samples with more connected particles, compared with the SR 1 route. It is possible to observe a major presence of sintering necks in samples prepared via the SR 3 route. As reported in the literature, during the two-state sintering method, excessive energy is given to the particles in the first heating step (T_3 = 1 600 °C in this study), which is used for diffusion of atoms along the second stage (T_2 = 1 500 °C), instead of particle boundary migration [13].

The microstructure of the sintered freeze-cast alumina sample formed via the fast route SR 4 is presented in Fig. 6. The SR 4 heat treatment produced samples with larger average pore sizes (Fig. 6), when compared to samples prepared with the conventional SR 1 (Fig. 5a-c) and two-step SR 3 (Fig. 5d-f) routes. The presence of large circular pores on the outer surface of the alumina samples, heat-treated with the SR 4 route (Fig. 6), suggest that non-isothermal

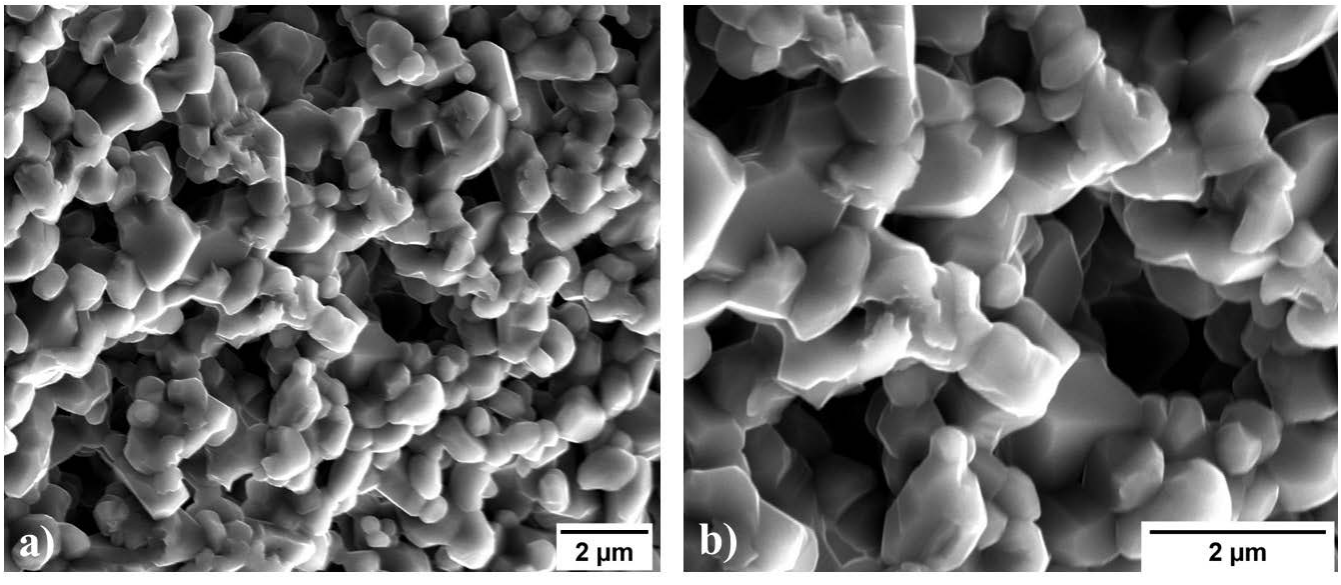

Fig. 4: SEM micrographs of alumina green bodies external surface.

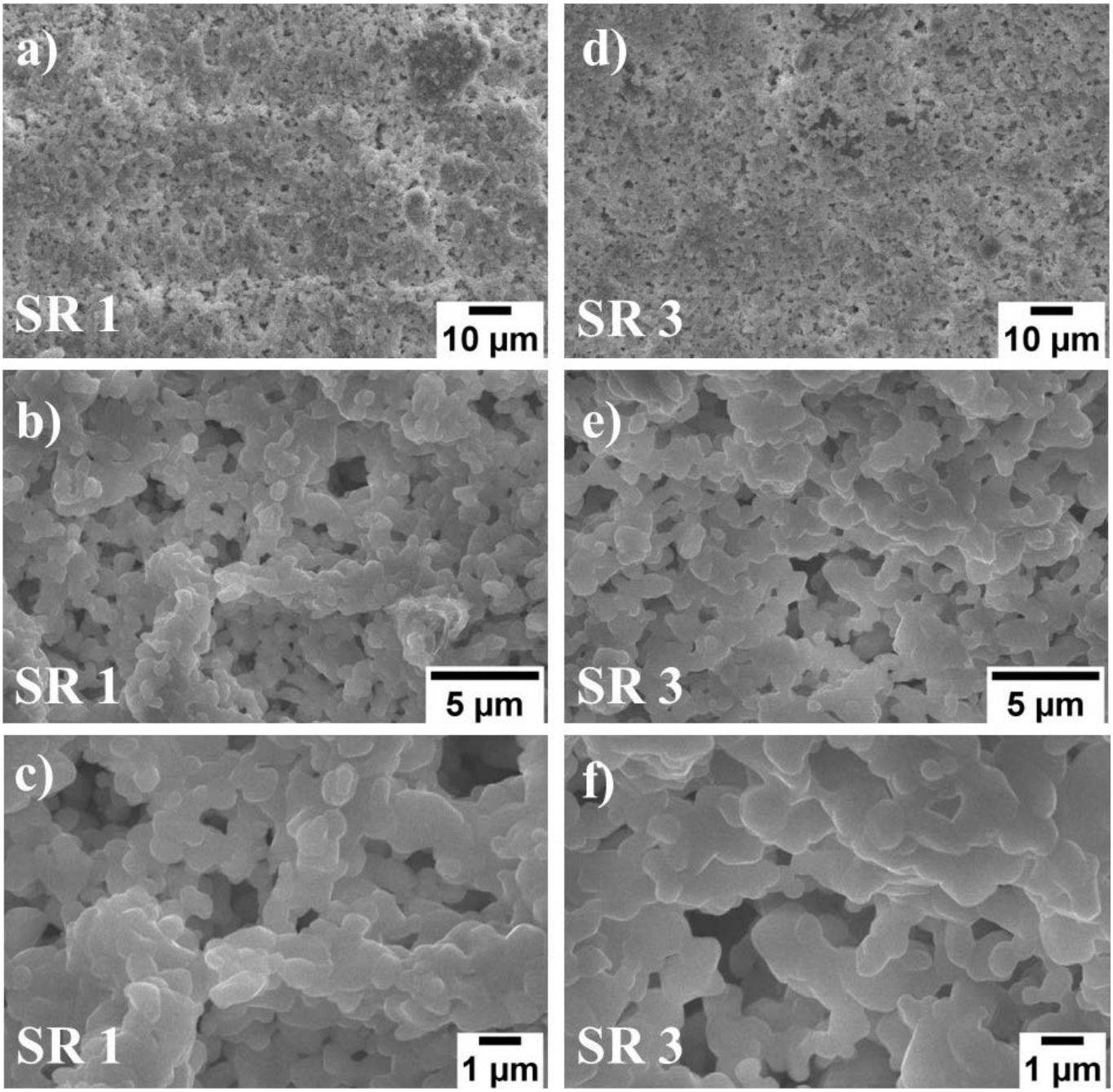

Fig. 5: SEM micrographs of the external surface of the freeze-cast tubular samples using the conventional SR 1 route with magnification of a) 1 000x, b) 5 000x and c) 10 000x and the two-step SR 3 heat treatment with magnification of d) 1 000x, e) 5 000x and f) 10 000x.

holding at 1 600 °C and subsequent cooling to room temperature defined the particles' size too quickly, not allowing enough time for them to settle into their equilibrium structures. Likewise, the heat treatment time was too short to allow pore shrinkage, leading to a smaller reduction in the diameter of pore channels of the green structure, even after the firing process, compared to other samples (leading to the sample with the smallest reduction of green body pore diameter after firing for the sintering routes evaluated in this work). The organization of the pore structure and well-defined channels shown in Fig. 6 suggests that the SR 4 heat treatment led to a small reduction in pore structure created by the solvent solification and lyophilization process compared to other methods. In addition, the fast route SR 4 was efficient in the sintering of the material, good coalescence of particles being observed compared to the green body (Fig. 4).

An analysis of the variation of the average particle diameter and average pore size of the outer surface of the green body and sintered samples was performed using Image J software and the results are shown in Fig. 7. The conventional sintering routes SR 1 and SR 2 exhibited the smallest average pore size and the largest average particle diameter among the analyzed samples. The final stage of conventional sintering of a solid solution is usually accompanied by rapid particle growth, as the driving forces for sintering and particles growth are comparable in order of magnitude, as demonstrated by Coble [26] and Chen

and Wang [13]. This phenomenon was more pronounced for samples sintered via the SR 2 route, since a higher temperature (1 600 °C) was used compared to the SR 1 route (1 500 °C). The use of higher temperatures in the conventional sintering route SR 2 enhanced the diffusion of aluminum ion and thus the sample densification, leading to the formation of ceramics with smaller average pore size [27].

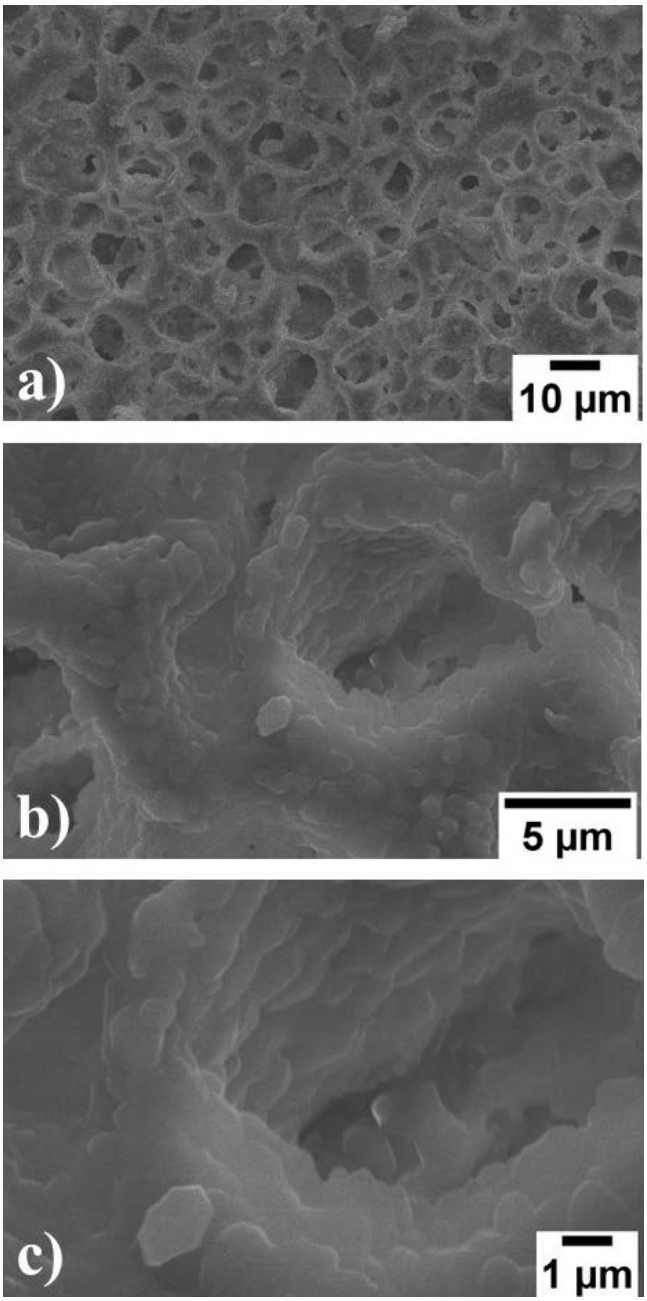

Fig. 6: SEM micrographs of the external surface of freeze-cast samples using the fast SR 4 heat treatment profile with magnification of d) 1 000x, e) 5 000x and f) 10 000x.

The similar average pore size presented by the green samples and the fast route SR 4 could be a result of the non-isothermal dwell at 1 600 °C and the insufficient time to allow green body densification. The rapid cooling from 1 600 °C to room temperature hinders the diffusion of alumina particles, leading to a smaller average particle diameter when compared to the conventional routes SR 1 and SR 2.

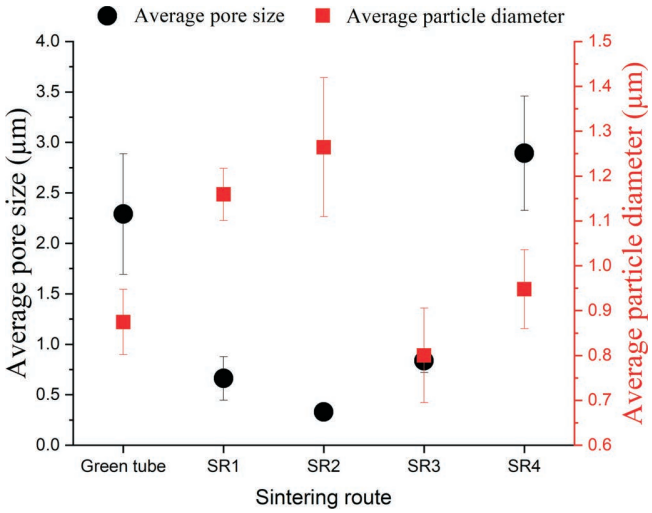

Fig. 7: Average pore size and alumina particle size of samples heat treated using different sintering routes.

Among the sintering routes studied, the two-stage route SR 3 was the one that resulted in samples with the smallest particle size, suggesting the occurrence of a "kinetic window" in the second stage of the heat treatment. The "*kinetic window*" corresponds to the interval between the temperatures required for sintering and particles growth [28,29]. This phenomenon can be assessed by exploring the difference between the activation energy for sintering and the activation energy for particle growth. In the first stage of sintering (T_3 = 1 600 °C), the temperature is high enough to reach the activation energy required for particle boundary mobility, allowing the alumina particles to form a particle boundary network throughout the bulk. Subsequently, the samples are cooled to a lower temperature (T_2 = 1 500 °C) where the activation energy is sufficient for particle boundary movement, resulting in sample densification. Thus, the cooling of the samples from T_3 to T_2 suppresses particle growth by "freezing" the microstructure, at the same time, the retention step in T_2 allows sample densification. The schematic representation of the difference between the two-stage route and conventional sintering is exhibited in Fig. 8. The results confirmed the behavior described by Chen and Wang [13], when they used two-stage heat treatment on nanocrystalline Y_2O_3 powders to prevent particle growth in the final stage of conventional sintering. Suppressing alumina particle growth in the final stage of sintering by applying a two-stage trajectory was successfully achieved by Bodišová *et al.* [12]; Bodišová *et al.* [14]; Galusek *et al.* [15] and Khan *et al.* [29].

The sintering routes assessed in this work resulted in samples whose pore structure is mainly composed of open pores, as shown in Fig. 9. Fig. 10 illustrates the effect of the green body shrinkage after sintering. The results indicate that the conventional sintering route SR 1 produced the sample with highest open porosity and smallest linear shrinkage. This behavior can be associated with the reduced pore mobility during sintering via the SR 1 route. In conventional sintering, particle growth occurs while the

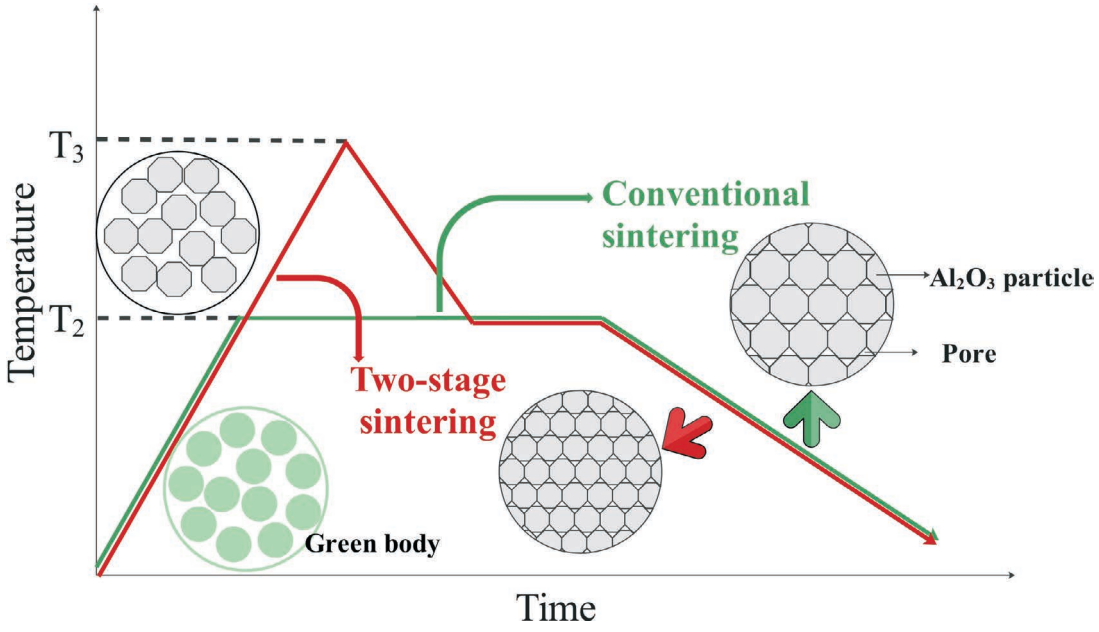

Fig. 8: Schematic illustration of the difference between conventional and two-stage sintering.

pores are located at particles boundaries. As the particles get larger, the distance between the pores and the particle boundaries increases. Pores get trapped inside the particles and it becomes more difficult for them to move [17].

An increase in the sintering temperature of conventional route from 1 500 °C (SR 1) to 1 600 °C (SR 2) resulted in a decrease of open porosity from 71.6 % to 55.1 %, which can be associated with the increase in diffusivity of aluminum ions at high temperatures, which reduces the pore channels between the particles. The open porosity of alumina samples heat-treated via the two-stage sintering route SR 3 is lower than those heat-treated via the conventional route SR 1, although the average pore size (Fig. 3) and the linear shrinkage of the two samples are similar. In the two-stage route, when the samples were heated to 1 600 °C, particle boundary migration was active and the pores became trapped. When the temperature was cooled to 1 500 °C, diffusion of atoms was active across particle boundaries, with no particle movement. The mass movement led to densification by using the two-stage SR 3 sintering route, as already predicted by the sintering profile proposed by Chen and Wang [13]. The samples sintered via the SR 4 route (fast sintering) showed an increase in open porosity (Fig. 4), when compared to the samples obtained with the conventional SR 2 route. The result can be attributed to the time that the samples were kept at 1 600 °C, which was 0 hours for the SR 4 route and 1 hour for the SR 2 route, thus indicating that the permanence at the temperature of 1 600 °C in SR 2 route favored sintering and enhanced sample densification.

From the scanning electron microscopy analysis, the open porosity and linear shrinkage results, the freeze-dried alumina microstructure is greatly affected by the sintering route and firing temperature. Therefore, it can be expected the sintering program would influence its mechanical properties as well. Fig. 11 shows the flexural strength of the samples as a function of open porosity after sintering. The results indicates that alumina samples heat-treated using the conventional route SR 1 exhibited the lowest flexural strength compared to the other samples. This behavior can be associated with the large number of pores (Fig. 4) present in this sample and also with its larger average alumina particle size (Fig. 3). Similarly, the alumina samples sintered via the conventional route SR 2 exhibited a considerable improvement in mechanical properties, which can be associated with their significant reduction in open porosity (Fig. 8). An empirical correlation proposed by Ryskewitsch [30], shown in Equation 3, describes the relationship between the porosity (p) and the mechanical strength (σ) of ceramic materials:

$$\sigma = \sigma_0 \exp(-\alpha p) \tag{3}$$

where σ_0 is the strength of the ceramic part with 0 % porosity and α a constant, and thus

$$\sigma \propto \exp(-p) \tag{4}$$

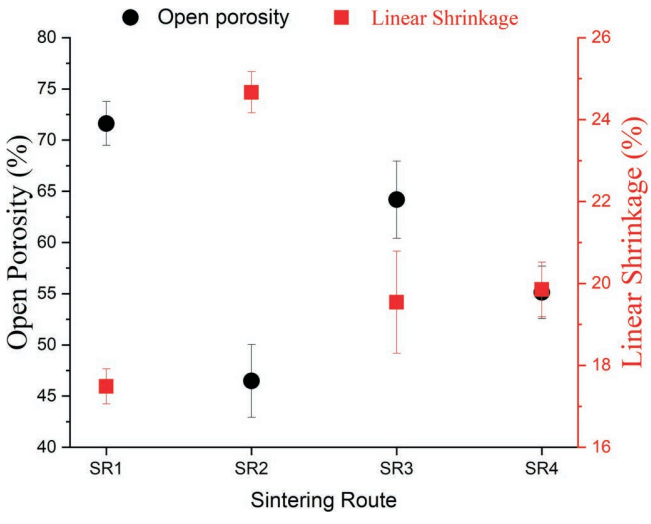

Fig. 9: Open porosity and linear shrinkage of alumina samples heat-treated via different sintering routes.

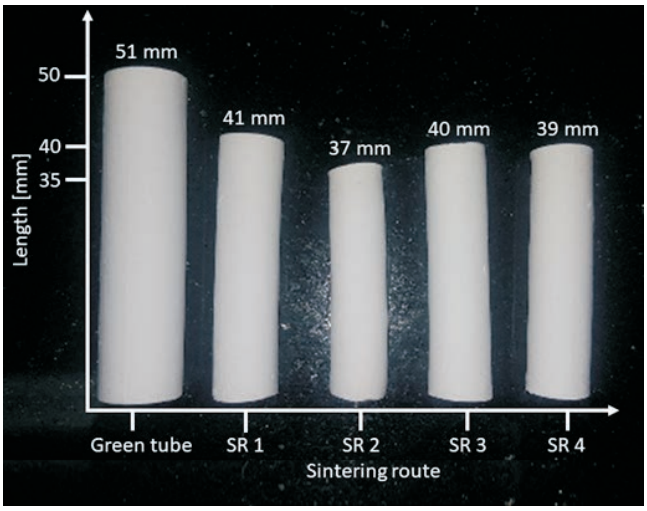

Fig. 10: Photo of alumina samples heat-treated using different sintering routes.

According to Equation 4, in ceramic materials with identical chemical composition, the increase in porosity causes a significant reduction in mechanical strenth. For samples sintered via the SR3 route, the improvement in flexural strength can be associated with the reduction in open porosity (Fig. 9) and also with the microstructural refinement caused by the two-stage sintering. The SR 3 heating led to a microstructure with smaller particles (Fig. 7), improving the mechanical strength of alumina samples. In the studies by Lóh *et al.* [20] and Khan *et al.* [29] on the influence of sintering treatment on the mechanical properties of alumina samples, the results also showed that two-step sintering improved the mechanical properties of the samples when compared to samples sintered using a conventional sintering program.

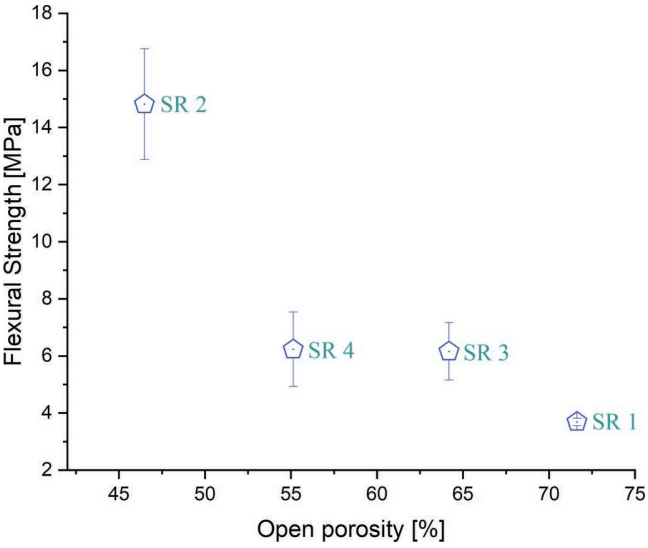

Fig. 11: Flexural strength versus open porosity of samples heat treated using different sintering routes.

The similar flexural strength of samples sintered via the fast route SR 4 and two-stage route SR 3 could be associated with the reduction of open porosity during the heating program. In sintering, the activation energy for particle growth is lower than for densification, since particle growth can occur as a result of low activation energy mechanisms such as surface diffusion, evaporation/condensation or particle boundary diffusion, whereas densification requires particle boundary diffusion. Therefore, coalescence of the particles can be active even at relatively low temperatures. With faster heating and subsequent cooling, there is a rapid passage through the low-temperature particle growth region, thus promoting densification in the fast route SR 4 [31].

The results of this work showed that the microstructure (average pore size, and average particle diameter) of alumina samples obtained by freeze-casting can be tailored by altering the sintering route. Depending on the application, the control of the pore network of a ceramic material is crucial for its performance. The structural parameters and mechanical properties of alumina samples obtained in this work suggest the potential of application of these supports in the manufacture of membranes for liquid and gas separation.

IV. Final Remarks

Samples prepared via the conventional sintering routes exhibited a larger average alumina particle diameter than samples obtained with the two-stage route (SR 3) and fast-sintering route (SR 4). In terms of particle growth inhibition, the two-step sintering proved to be more efficient than the other sintering methods studied.

The conventional (SR 1) and two-stage (SR 3) sintering routes produced samples with similar pore sizes, while fast sintering (SR 4) resulted in an average pore size about six times larger than conventional sintering.

The increase in flexural strength of the heat-treated samples using the SR 2 route is attributed to a larger reduction of open porosity.

Acknowledgments

The authors thank Petrobras,CAPES-PROEX and CNPq for their financial support of this study. We thank the INCT-Acqua for the technical support in the lyophilization process and the UFMG Microscopy Center for the support given to this research to obtain the SEM images.

References

1 Deville, S.: Freeze-casting of porous ceramics: A review of current achievements and issues, *Adv. Eng. Mater.*, **10**, [3], 155 – 169, (2008)
doi: https://dx.doi.org/10.1002/adem.200700270

2 Pagano, E., Chinelatto, A.S.A., Chinelatto, A.L.: Freeze casting process for the generation of graded porosity in Al_2O_3 ceramics, *Ceramica*, **66**, [377], 65 – 73, (2020).
doi: https://doi.org/10.1590/0366 – 69132020663772690.

3 Barbosa, T.L.A., Silva, F.M.N., Barbosa, A.S., Lima, E.G., Rodrigues, M.G.F.: Synthesis and application of a composite NaA zeolite/gamma-alumina membrane for oil-water separation process, *Ceramica*, **66**, 137 – 144 (2020).
doi: https://dx.doi.org/10.1590/0366 – 69132020663782820.

4 Hyun, S.H., Kim, G.T.: Synthesis of ceramic microfiltration membranes for oil/water separation, *Sep. Sci. Technol.*, **32**, [18], 2927 – 2943, (1997).
doi: https://doi.org/10.1080/01496399708000788.

5 Kabir, S.M., Minhaj, I.T., Ashrafi, A.E., Hossain, M.M.: Influence of sintering routes on the structure and indentation

hardness of nano α-Al_2O_3 particles, *IJAENT*, **9**, 2347 – 6389, (2014).

6 Wu, T., Wang, B., Lu, Z., Zhou, R., Chen, X.: Alumina-supported AlPO-18 membranes for CO_2/CH_4 separation, *J. Membr. Sci.*, **471**, 338 – 346, (2014). doi: https://dx.doi.org/10.1016/j.memsci.2014.08.035.

7 Liu, R., Xu, T., Wang, C.: A review of fabrication strategies and applications of porous ceramics prepared by freeze-casting method, *Ceram. Int.*, **42**, 2907 – 2925, (2016). doi: https://dx.doi.org/10.1016/j.ceramint.2015.10.148.

8 German, R.M.: *Thermodynamics of sintering*, San Diego State University, In book: Sintering of advanced materials, Woodhead Publishing, 3 – 32, 2010.

9 Rahaman, M.N.: *Ceramic Processing and Sintering*, Second Edition, New York, CRC Press, 550, 2017.

10 Callister, W.D. Jr., Rethwisch, D.G.: Wiley, Salt Lake City, Eighth edition: *Materials Science and Engineering*, 2010.

11 Awotunde, M.A., Adegbenjo, A.O., Obadele, B.A., Okoro, M., Shongwe, B.M., Olubambi, P.A.: Influence of sintering methods on the mechanical properties of aluminium nanocomposites reinforced with carbonaceous compounds: A review, *J. Mater. Res. Technol*., **8**, [2], 2432 – 2449, (2019). doi: https://doi.org/10.1016/j.jmrt.2019.01.026.

12 Bodišová, K., Galusek, D., Švančárek, P., Pouchlý, V., Maca, K.: Grain growth suppression in alumina via doping and two-step sintering, *Ceram. Int*., **41**, [9], 11975 – 11983, (2015). doi: https://doi.org/10.1016/j.ceramint.2015.05.162.

13 Chen, I.W., Wang, X.H.: Sintering dense nanocrystalline ceramics without final-stage grain growth, *Nature*, **9**, 168 – 171, (2000). doi: https://doi.org/10.1038/35004548.

14 Bodišová, K., Sajgalik, P., Galusek, D., Svancarek, P.: Two-stage sintering of alumina with submicrometer grain size, *J. Am. Ceram. Soc.*, **90**, 330 – 332, (2007). doi: https://doi.org/10.1111/j.1551 – 2916.2006.01408.x.

15 Galusek, D., Ghillányová, K., Sedláček, J., Kozánková, J., Šajgalík, P.: The influence of additives on microstrucutre of sub-micron alumina ceramics prepared by two-stage sintering, *J. Eur. Ceram.*, **32**, 1965 – 1970, (2012). doi: https://doi.org/10.1016/j.jeurceramsoc.2011.11.038

16 Prajzler, V., Salamon, D., Maca, K.: Pressure-less rapid rate sintering of pre-sintered alumina and zirconia ceramics, *Ceram. Int.*, **44**, 10840 – 10846, (2018). doi: https://doi.org/10.1016/j.ceramint.2018.03.132.

17 Kang, S.L.: What we should consider for full densification when sintering, *Materials*, **13**, (2020). doi: https://doi.org/10.3390/ma13163578.

18 Esposito, V., Traversa, E.: Design of electroceramics for solid oxides fuel cell applications: playing with ceria, *J. Am. Ceram.*, **91**, 1037 – 1051, (2008).

19 Isobe, T., Ooyama, A., Shimizu, M., Nakajima, A.: Pore size control of Al_2O_3 ceramics using two-step sintering, *Ceram. Int.*, **38**, 787 – 793, (2012). doi: https://doi.org/10.1016/j.ceramint.2011.08.005.

20 Lóh, N.J., Simão, L., Jiusti, J., Arcaro, S., Raupp-pereira, F., De Noni Jr., A., Montedo, O.R.K.: Densified alumina obtained by two-step sintering: impact of the microstructure on mechanical properties, *Ceram. Int.*, **46**, 12740 – 12743, (2020). doi: https://doi.org/10.1016/j.ceramint.2020.02.042.

21 Lóh, N.J., Simão, L., Faller, C.A., De Noni Jr, A., Montedo, O.R.K.: A review of two-step sintering for ceramics, *Ceram. Int.*, **42**, 12556 – 12572, (2016). doi: https://dx.doi.org/10.1016/j.ceramint.2016.05.065

22 Xu, T., Wang, C.-A.: Effect of two-step sintering on microhoneycomb $BaTiO_3$ ceramics prepared by freeze-casting process, *J. Eur. Ceram.*, **36**, 2647 – 2652, (2016). doi: https://doi.org/10.1016/j.jeurceramsoc.2016.03.032.

23 A.S.T.M. B962 – 17, Standard test methods for density of compacted or sintered powder metallurgy (PM) products using Archimedes' principle, 2017.

24 A.S.T.M. C20 – 00, Standard test methods for apparent porosity, water absorption, apparent specific gravity, and bulk density of burned refractory brick and shapes by boiling water, 2015.

25 Wit, P., Daalen, F.S., Benes, N.E.: The mechanical strength of a ceramic porous hollow fiber, *J. Membr. Sci.*, **524**, 721 – 728, (2017). doi: https://dx.doi.org/10.1016/j.memsci.2016.11.047.

26 Coble, R.L.: Sintering crystalline solids. I. Intermediate and final state diffusion models. *J. Appl. Phys*., **32**, 787 – 792, (1961). doi: https://dx.doi.org/10.1063/1.1736107.

27 Silva, L.O., Vasconcelos, D.C.L., Nunes, E.H.M., Caldeira, L., Costa, V.C., Musse, A., Hatimondi, S.A., Nascimento, J.F., Grava, W., Vasconcelos, W.L.: Processing, structural characterization and performance of alumina supports used in ceramic membranes, *Ceram. Int.*, **38**, 1943 – 1949, (2012). doi: https://doi.org/10.1016/j.ceramint.2011.10.025.

28 Pouchly, V., Maca, K.: Sintering kinetic window for yttria-stabilized cubic zirconia vaclav, *J. Eur. Ceram*., **36**, 2931 – 2936, (2016). doi: https://dx.doi.org/10.1016/j.jeurceramsoc.2015.12.044.

29 Khan, U.A., Hussain, A., Shah, M., Shuaib, M., Qayyum, F.: Investigation of mechanical properties based on grain growth and microstructure evolution of alumina ceramics during two step sintering process. *IOP Conf*., 146, (2016). doi: https://dx.doi.org/10.1088/1757 – 899X/146/1/012046.

30 Pan, Y., Li H., Liu, Y., Liu, Y., Hu, K., Wang, N., Lu, Z., Liang, J., He, S.: Effect of holding time during sintering on microstructure and properties of 3D printed alumina ceramics, *Front. Mater.*, **7**, [54], (2020). doi: https://dx.doi.org/10.3389/fmats.2020.00054.

31 Biesuz, M., Grasso, S., Sglavo, V.M.: What's new in ceramics sintering? A short report on the latest trends and future prospects, *Curr. Opin. Solid State Mater. Sci.*, **24**, [5], 100868, (2020). doi: https://doi.org/10.1016/j.cossms.2020.100868